Figure S1

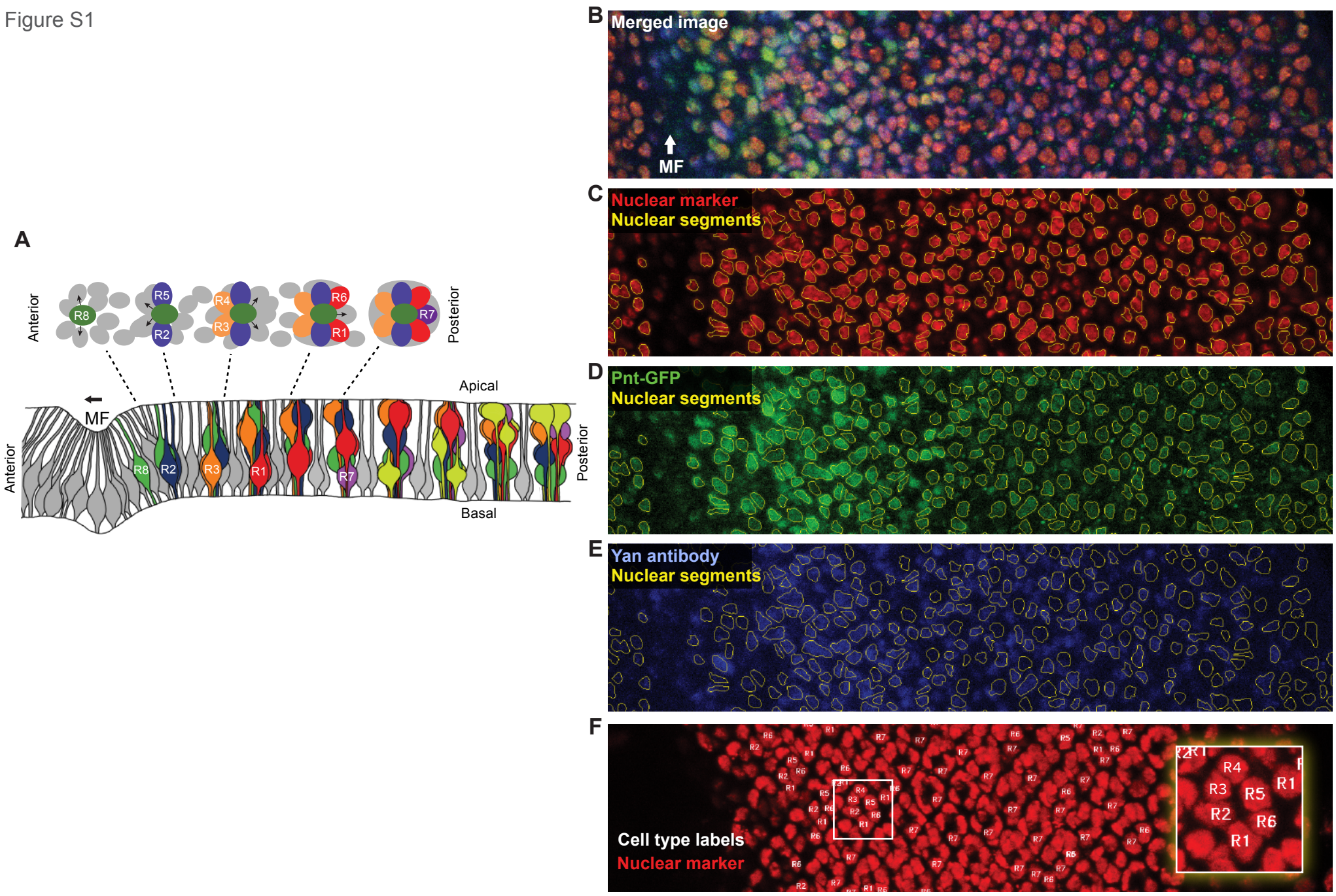

Fig. S1. Identification of cell nuclei in eye discs.

(A) Schematic cross-sectional view along the anteroposterior axis of an eye disc, showing the epithelial invagination that marks the MF and the assembling clusters of differentiated cells forming ommatidia. Note the dynamic and characteristic apical-basal positions of nuclei from progenitor cells (grey), R cells (various colors), and cone cells (light green). Shown above is a apical-basal view of five ommatidia sampled at different locations along the anteroposterior axis. The relative positions of progenitor and R cell nuclei are highly stereotyped in this plane. Arrows denote signals transmitted from the R8 to neighboring progenitor cells and transduced via the RTK – Ras – MAPK pathway. Adapted from (Peláez et al., 2015).

(B-E) Quantitative analysis pipeline showing microscopy and segmentation of one representative eye disc. Shown is a partial cross-section of a confocal z-stack with the merged channels (B) and separate fluorescence channels for Histone-RFP (C), Pnt-GFP (D), and Yan antibody (E). MF marks the location of the MF. Yellow lines depict nuclear contours segmented by FlyEye Silhouette.

(F) Manual annotation of R-cell types. Image shows a projection of His-RFP fluorescence across the Z-sections spanning R cell nuclei. The region imaged is identical to that shown in (B-E). The R-cell types are documented and are labelled as shown. The inset shows an ommatidium magnified to see nuclear positions.

Figure S2

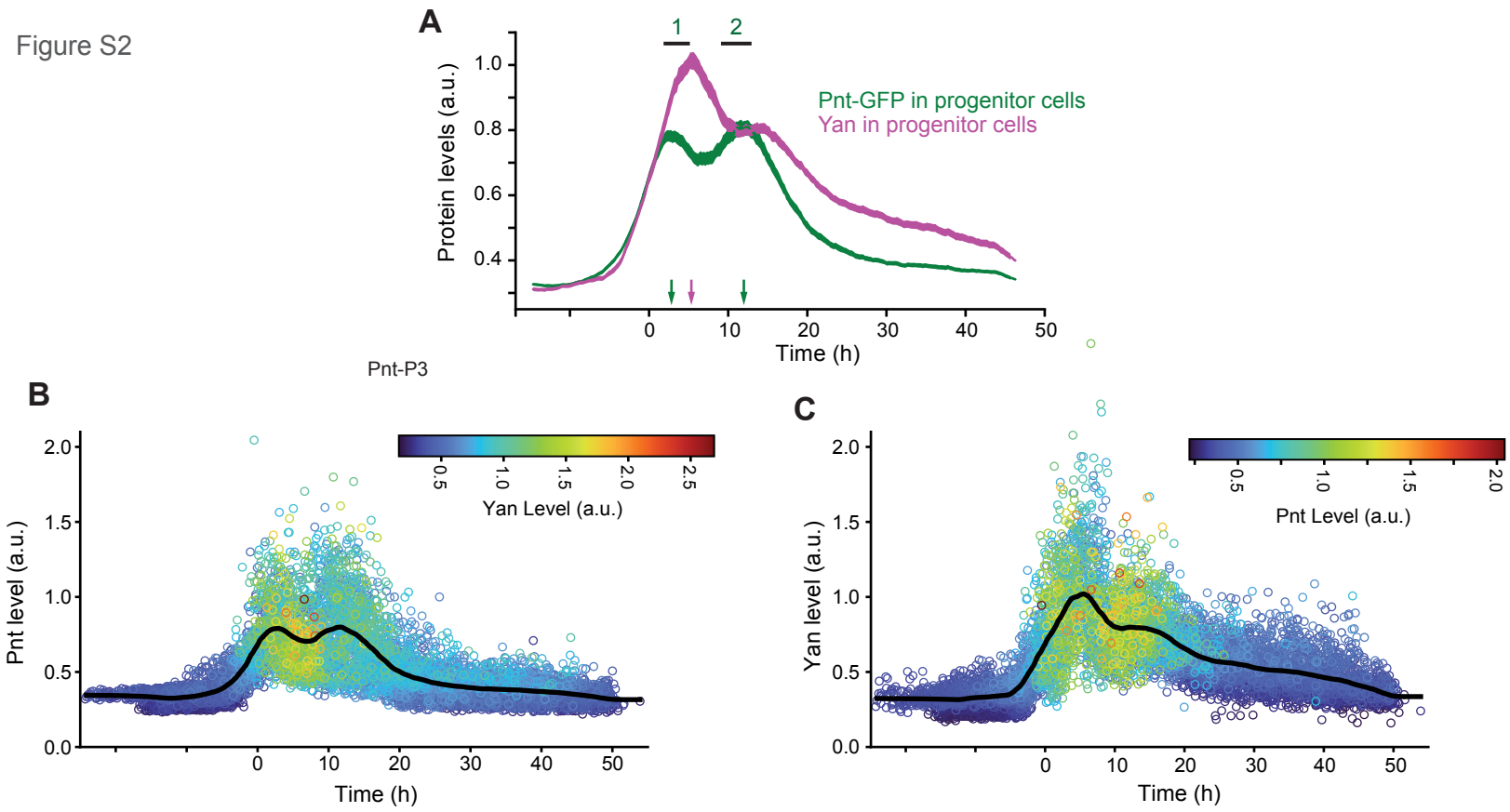

Fig. S2. Pnt-GFP and Yan expression in progenitor cells.

(A) Line averages of Pnt-GFP (green) and Yan (magenta) levels in progenitor cells. Lines are smoothed moving averages across 500 sequential progenitors, shaded regions are 95% confidence intervals. Arrows indicate the times at which local maxima occur. Note the peaks of Pnt and Yan expression take place sequentially in progenitor cells.

(B, C) Expression levels of Pnt-GFP (B) and Yan (C) in individual progenitor cells, color-coded in accordance with the expression level of the complementary transcription factor, as shown at the right of each panel. Datapoints are arranged such that those with higher levels of the complementary transcription factor are displayed in front. Lines are smoothed moving averages across 500 sequential progenitor cells.

Figure S3

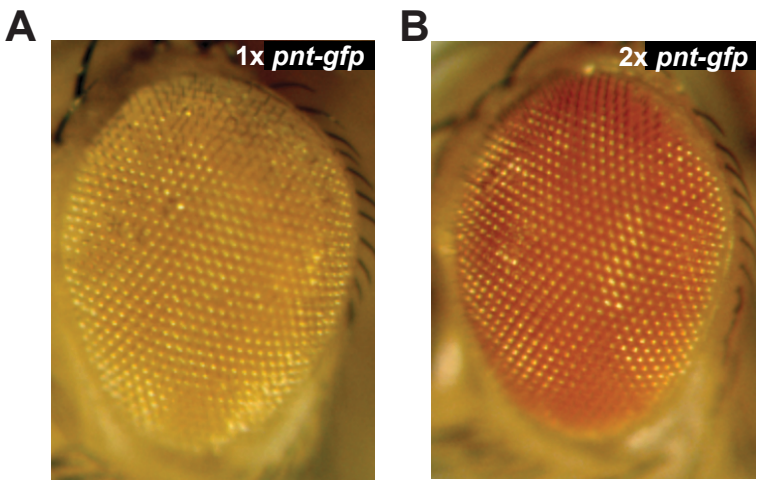

Fig. S3. Characterization of Pnt-GFP.
Adult eyes of flies carrying **(A)** one or **(B)** two copies of the *pnt-gfp* transgene in a *pnt* null mutant background.

Figure S4

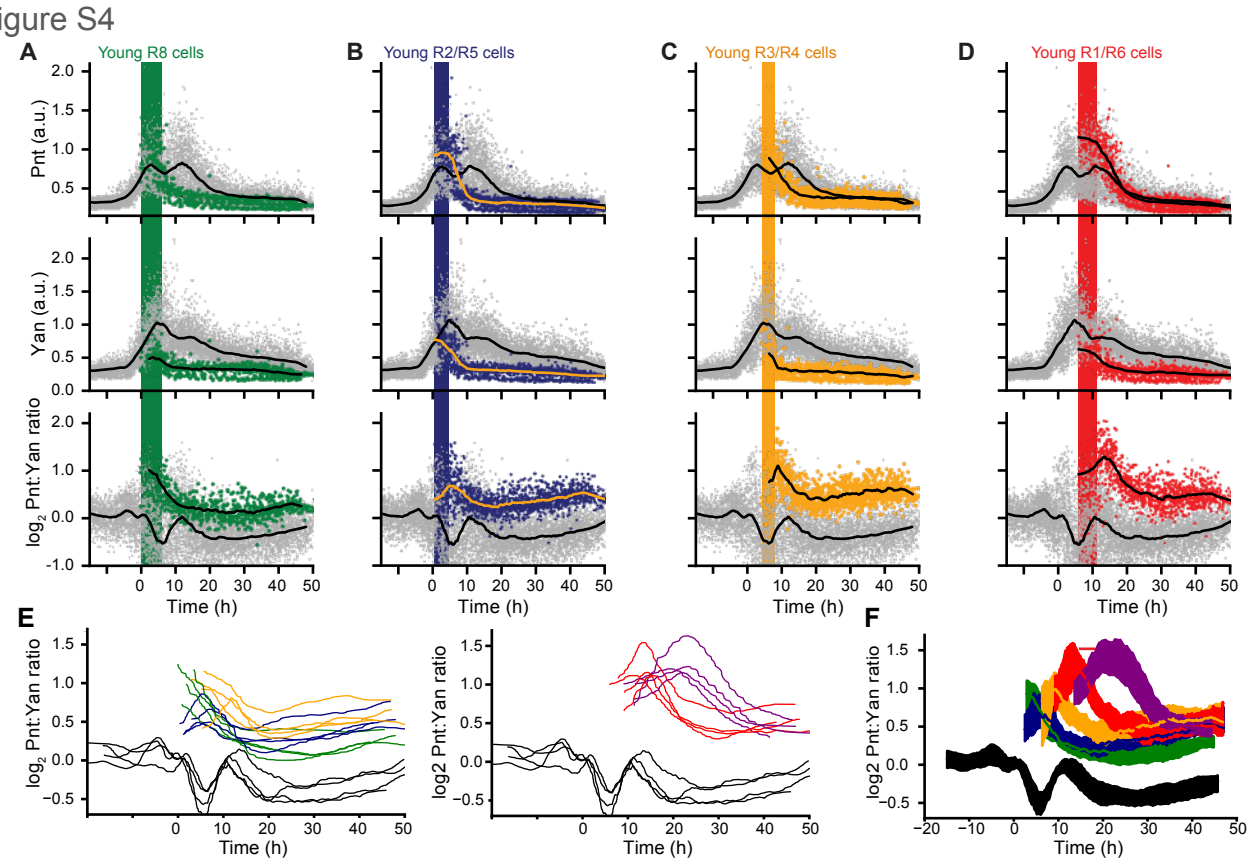

Fig. S4. Expression dynamics for various eye cell types.

(A-D) Pnt-GFP and Yan protein levels, and the $\log_2$-transformed Pnt/Yan ratio for individual progenitor (grey), and R8 cells (**A**), R2/R5 cells (**B**), R3/R4 cells (**C**), and R1/R6 cells (**D**) over developmental time. Progenitor cells are present across all time (grey arrow) while R cells arise later in time (colored arrows). Solid black lines are smoothed moving averages across 250 and 75 individual nuclei for progenitor and R cells, respectively. Black bars labeled 1 and 2 denote the two peaks of Pnt-GFP in progenitor cells. Shaded vertical stripes highlight these two regions, which coincide with transition of progenitor to various R fates.

(E) Moving averages for the $\log_2$-transformed Pnt/Yan ratio for progenitor (grey), R8 cells (green), R2/R5 cells (blue), R3/R4 cells (orange), R1/R6 cells (red), and R7 cells (purple) over developmental time from individual WT replicate discs. **(F)** Moving averages for the $\log_2$-transformed Pnt/Yan ratio for progenitor (grey), R8 cells (green), R2/R5 cells (blue), R3/R4 cells (orange), R1/R6 cells (red), and R7 cells (purple) from three replicate WT discs, along with 95% confidence interval of the mean for each cell type obtained from two-stage hierarchical bootstrapping approach that first subsamples the independent discs, then subsamples the cell measurements within them.

Figure S5

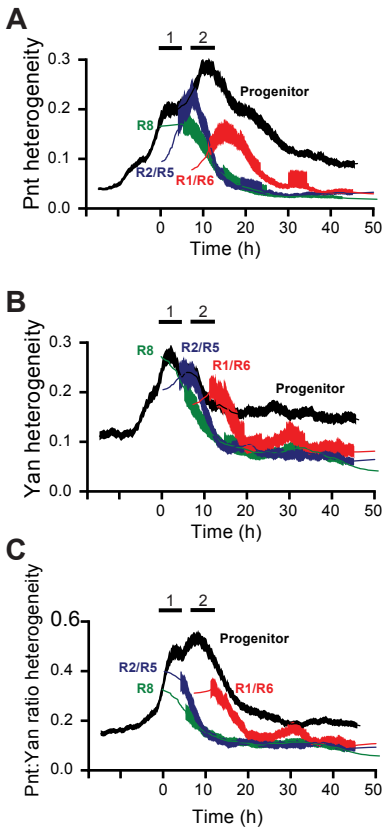

Fig. S5. Heterogeneity of Yan and Pnt expression.

Cell-to-cell expression heterogeneity of Pnt-GFP **(A)**, Yan **(B)**, and the $\log_2$-transformed Pnt/Yan ratio **(C)**. Heterogeneity was estimated by de-trending fluctuations about a moving average of 250 sequential cells as described (Paleaz 2015). Lines shown are moving averages of 250 sequential fluctuations. Shaded regions are 95% confidence intervals. Colors denote cell type.

Figure S6

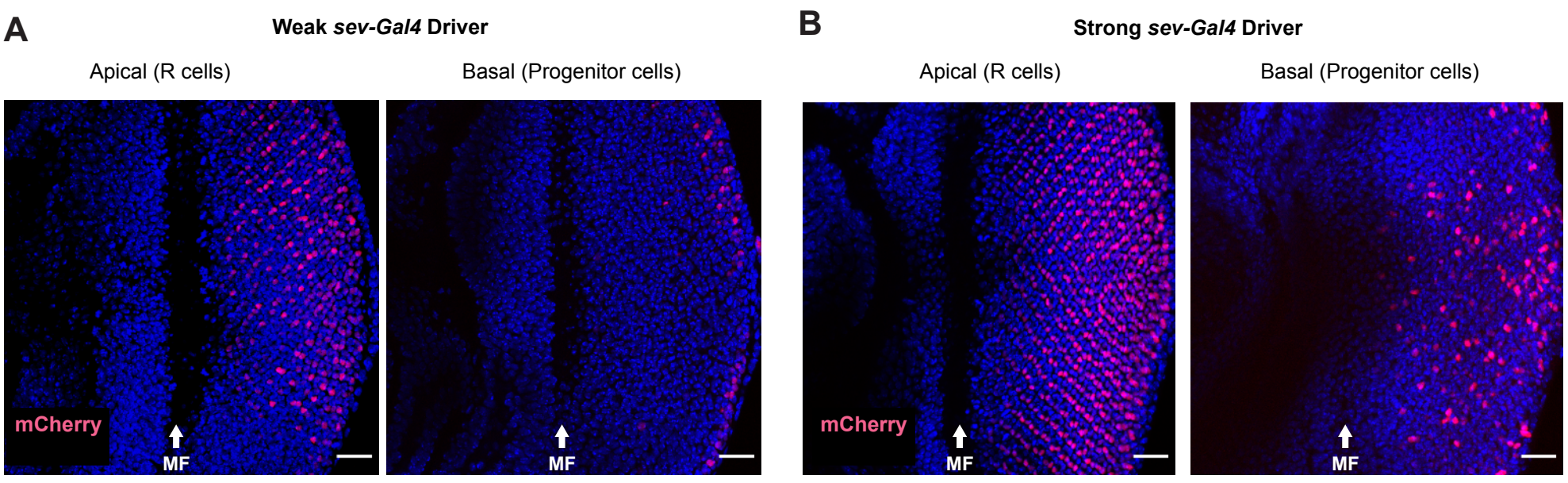

Fig. S6. *Sev-Gal4* drives UAS transgene expression in subsets of progenitor cells.

Projection of *sev-Gal4>UAS-NLS-mCherry* protein fluorescence (red) and DAPI (blue) in apical z-slices containing R-cell nuclei and basal z-slices containing progenitor cell nuclei. Anterior is left and MF is morphogenetic furrow. Scale bars denote 20 μm. **(A)** Expression from a weak *sev-Gal4* driver. **(B)** Expression from a strong *sev-Gal4* driver. When expressed from the weak driver, mCherry is predominantly limited to R7, R3, and R4 cells. When expressed from the strong driver, mCherry is also detected in some progenitor cells.

Figure S7

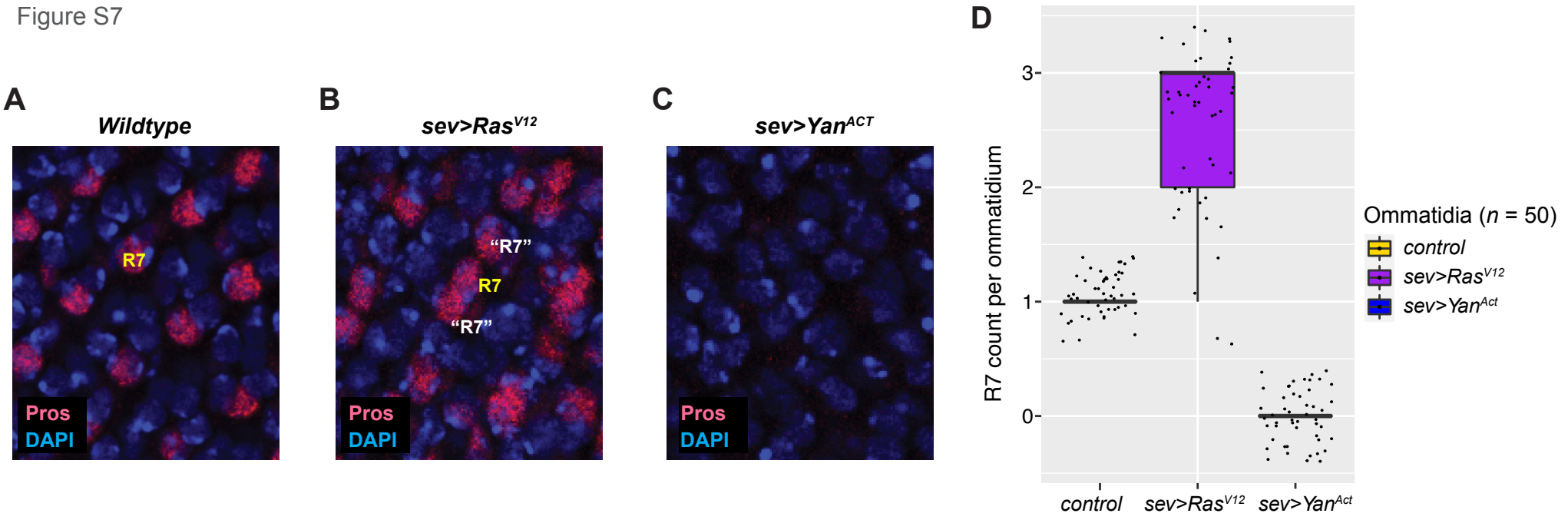

Fig. S7. Fate specification errors in *sev>Ras^{V12}* and *sev>Yan^{ACT}*.

Prospero (Pros) protein fluorescence in a region of the eye disc where ommatidia have recruited cells to form R7 cells. Pros is specifically expressed in R7 cells. **(A)** Ommatidia in wildtype eye disc, which have one Pros-positive cell per ommatidium. **(B)** Some ommatidia in a *sev>Ras^{V12}* eye disc have ectopic R7 cells labelled "R" (white font) that are Pros-positive and located beside the endogenous R7 cells (labeled with yellow font). **(C)** Ommatidia from a *sev>Yan^{ACT}* eye disc have no Pros-positive cells, indicating that they lack R7 cells. **S7D**. Number of R7 cells positive for the R7 marker Prospero in individual mature ommatidia of wildtype, *sev>Ras^{V12}* and *sev>Yan^{ACT}* discs (*n* = 50 ommatidia analyzed for each group across 3 replicate discs). Boxplots are median and quartiles.

Figure S8

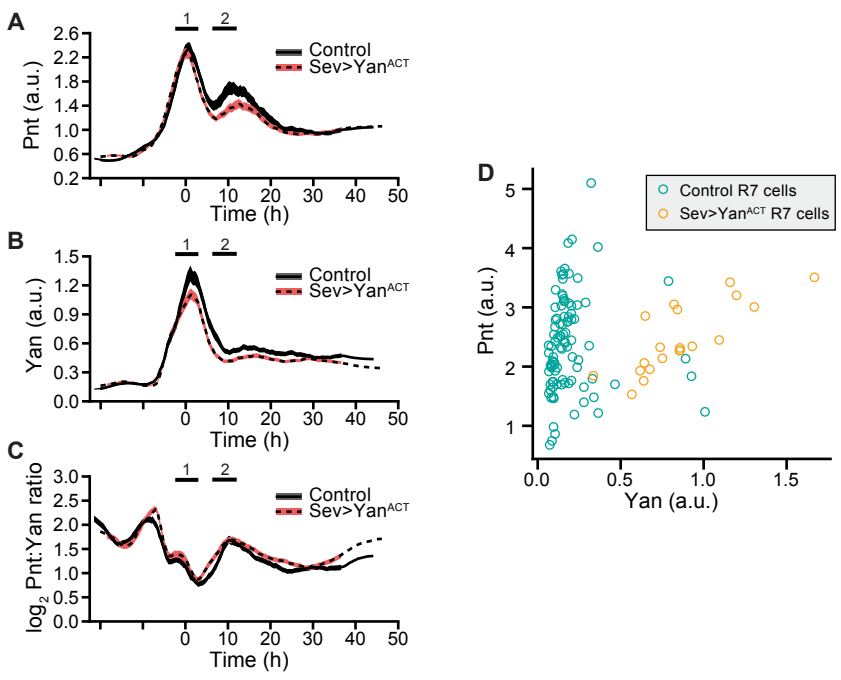

Fig. S8. Yan^{ACT} has no effect on the Pnt/Yan ratio in progenitor cells but does alter Yan levels in R7 cells.

(A-C) Effect of *sev>Yan^{ACT}* expression on Pnt-GFP (A), Yan (B), and the $\log_2$-transformed Pnt/Yan ratio (C) in progenitor cells over time. Lines are moving averages across 250 sequential cells. Shaded regions are 95% confidence intervals. Black lines denote wildtype cells. Red lines denote *sev>Yan^{ACT}* cells. **(D)** Joint distribution of Pnt and Yan levels among R7 cells sampled from the region spanning 15 to 20 h of developmental time. The *sev>Yan^{ACT}* R7 cells show higher Yan levels ($P<0.001$, one-tailed Mann-Whitney U test), while Pnt levels are indistinguishable from wildtype ($P=0.4$, KS 2-sample test).

Figure S9

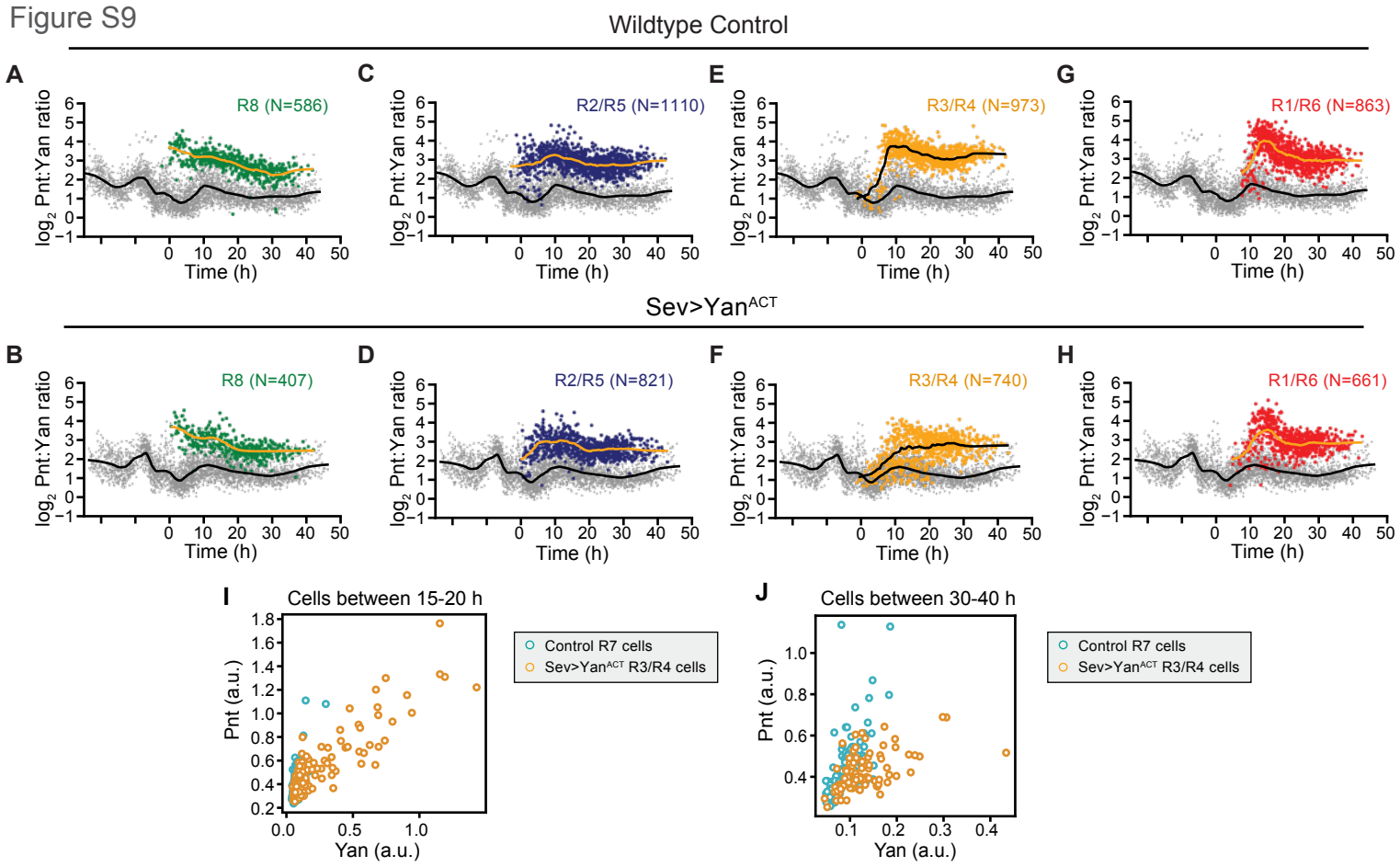

Fig. S9. Yan^{ACT} has a weak effect on the Pnt/Yan ratio in R3/R4 cells.

The log_2-transformed Pnt/Yan ratio for individual R cells (dots) and their moving line averages (black lines) over developmental time in wildtype **(A,C,E,G)** and *sev>Yan^{ACT}* eyes **(B,D,F,H)**. The moving line average

for progenitor cells (black lines) is also shown in each plot. Black bars labeled 1 and 2 denote the two peaks of Pnt-GFP in progenitor cells, which coincide with transition of progenitor to various R fates. Various R cell types are shown, R8 **(A,B)**, R2/R5 **(C,D)**, R3/R4 **(E,F)**, and R1/R6 **(G,H)**. **S9 (I, J)** Joint distribution of Pnt and Yan levels among R3/R4 cells sampled from the region spanning 15 to 20 h (**I**) and 30 to 40 h (**J**) of developmental time. In both cases, a KS 2-sample test on the log_2 Pnt:Yan ratio yields $p<$ 0.00001.

Figure S10

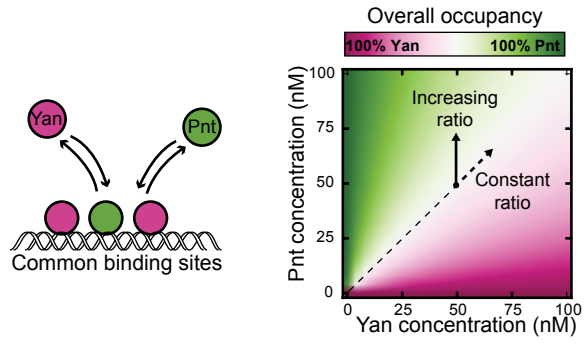

Fig. S10. A simple equilibrium model of Yan / Pnt competition for DNA binding sites.

Schematic of a simple two-species competitive binding model (left), alongside theoretical Pnt site occupancy as a function of transcription factor abundance (right). Equivalent binding affinities are used for illustrative purposes. Color scale reflects overall Pnt site occupancy. A diverging scale was used because all sites are fully saturated at total transcription factor concentrations above 1 nM. Under the range of conditions shown, this implies that Yan occupies all sites left vacant by Pnt. Simultaneous proportional increases in absolute abundance of both species have minimal impact on Pnt occupancy (dashed arrow), while varying ratio confers gradual change in occupancy (solid arrow).

Figure S11

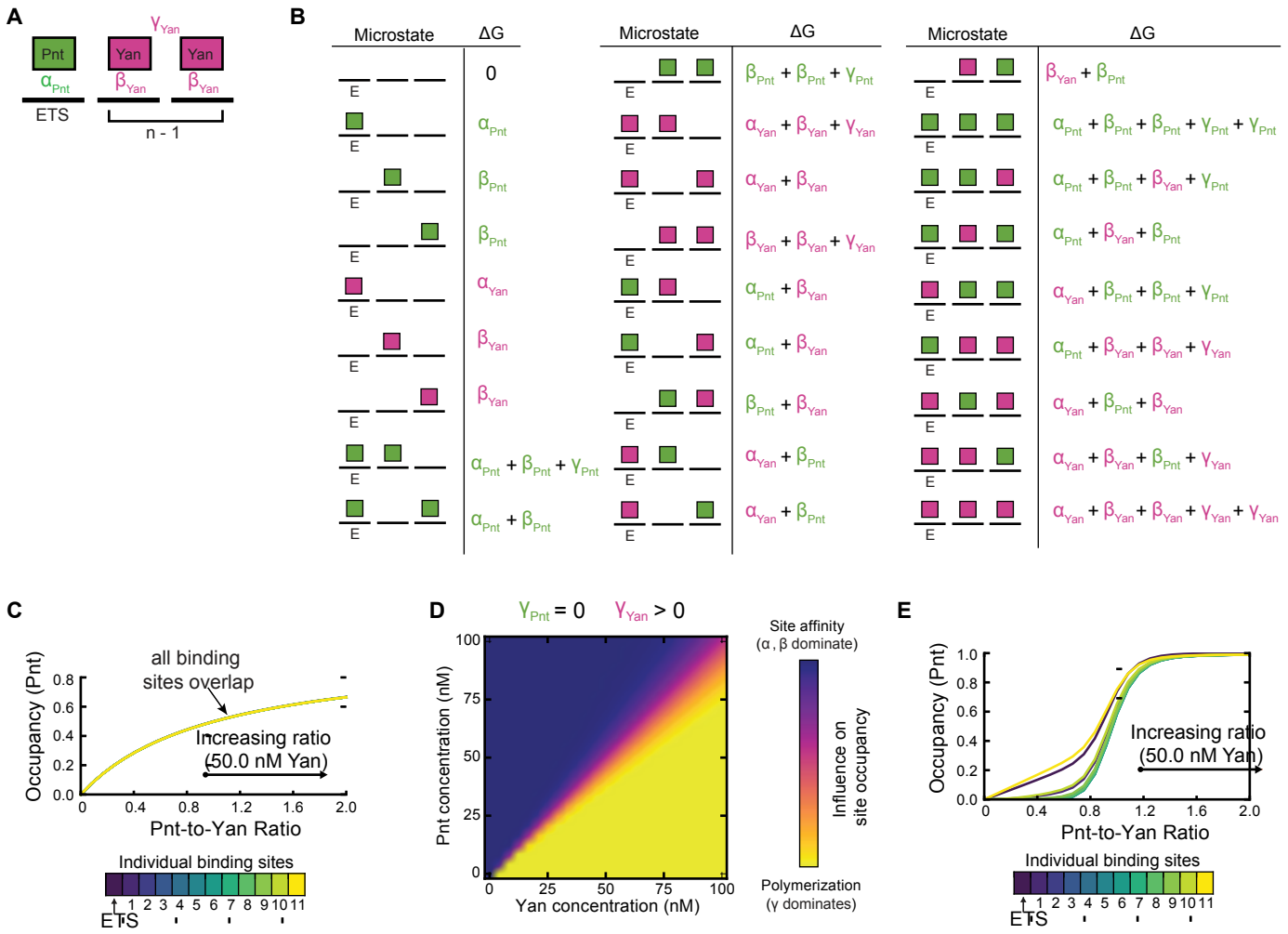

Fig. S11. Cooperative DNA-binding by Yan sensitizes occupancy of DNA sites to the Pnt/Yan ratio.

(A) Summary of thermodynamic interactions within one microstate of a cis-regulatory element containing one ETS site and two non-ETS sites. Solid black lines represent individual binding sites. Green and magenta rectangles denote Pnt and Yan molecules. Example thermodynamic potentials of strong ETS-binding, weak non-ETS binding, and polymerization interactions are denoted by α_{Pnt}, β_{Yan}, and γ_{Yan}, respectively. For this microstate, $\alpha_P(k)$=1 and $\alpha_Y(k)$=2.

(B) Enumeration of all possible microstates for a cis-regulatory element of length 3 in which only the first site carries the ETS designation. Solid black lines denote binding sites, green and magenta rectangles denote bound Pnt and Yan molecules. The cumulative thermodynamic potentials of each microstate, ΔG_k, are listed beside each graphical depiction.

(C) Pnt occupancy of individual binding sites as a function of Pnt/Yan ratio in the absence of Yan polymerization. Contours correspond to a vertical path traversed across Figure 6A at a fixed Yan concentration of 50 nM. All binding sites behave similarly.

(D) Relative thermodynamic contributions of binding site affinity versus polymerization to microstate statistical frequencies as a function of Pnt and Yan concentration. For each point in the plane, the influence of site affinity was calculated by weighting the sum of all ETS and non-ETS thermodynamic potentials for each microstate by the statistical frequency of the corresponding microstate. The influence of polymerization was similarly determined. The color scale reflects the relative magnitude of these two summations, normalized by limits of zero and complete polymerization.

(E) Pnt occupancy of individual binding sites as a function of Pnt/Yan ratio when Yan polymerizes. Contours correspond to a vertical path traversed across Figure 6B at a fixed Yan concentration of 50 nM. Line colors reflect binding site positions within the cis-regulatory element. Sites at intermediate distances from the strong ETS site (green lines) transition at higher ratios than those nearest and furthest from the strong ETS site (blue and yellow lines).

Table S1. Accuracy of cell-type identification

Cell Type Scored	Cell Type Marker	Sample Size (*n*)	% Correct Type Assignment
Progenitors	Elav (-)	462	99.8
All mature Rs	Elav (+)	258	99.2
R8	Sens	106	97.2
R2/R5	Rough	162	99.4
R3/R4	Rough	142	100.0
R7	Pros	104	99.0